Second-order dielectric stopping of ions in a free-electron gas

D. G. Arbó, M. S. Gravielle, and J. E. Miraglia

*Instituto de Astronomía y Física del Espacio, Consejo Nacional de Investigaciones Científicas y Técnicas, Casilla de Correos 67,
Sucursal 28, 1428 Buenos Aires, Argentina
and Departamento de Física, FCEyN, Universidad de Buenos Aires, Argentina*

The energy lost by a heavy projectile, with charge Z_P, moving in a free-electron gas is studied within the framework of the dielectric formalism. In this model, the potential induced by the projectile is expanded in a perturbative series, and terms up to second order in Z_P are conserved. The obtained quadratic potential is expressed as a function of the first-order dielectric response or Lindhard dielectric function. We apply the formalism to the calculation of stopping for different fixed charges (protons, neutral hydrogen, and antiprotons) moving in aluminum. Energy-loss distributions are investigated, and in the case of antiprotons, the second-order term is modified to avoid negative probabilities. The total stopping power, calculated taking into account the inner-shell contribution and different charge states in equilibrium, is compared with experimental data. The induced electronic density is also studied, and results agree with those derived from the density-functional theory.

I. PRELIMINARY

In a previous work [1], we calculated the first-order stopping power for a fast ion with charge Z_P moving through a free-electron gas (FEG). We worked within the framework of two different formulations, namely the binary collisional formalism (BCF), also called kinetic theory [2], and the dielectric formulation (DF) [3]. While the first formalism only describes the energy loss by binary collisions, the second one provides the energy lost in both single-particle and collective processes, without separating its contributions. In both models, the first perturbative order of the stopping power depends on Z_P^2, being therefore insensitive to the sign of projectile charge; i.e., protons and antiprotons yield the same results. To study the experimentally observed dependency of the energy loss on the sign of Z_P, in Ref. [4] we calculated the second-order stopping power within the BCF. It was evaluated by means of the second-order Born approximation to describe the electronic transitions, but still using the first-order induced potential. As derived within the BCF, this approximation only takes into account the binary mechanism of energy loss, therefore the use of the DF is necessary to consider the second-order collective effects.

The aim of the present work is to investigate the second-order stopping power within the DF, which includes both binary excitations and collective oscillations. In the DF, the Z_P^3 correction of the stopping is obtained by expanding the potential induced by the projectile up to second order in Z_P. This quadratic potential, which was developed by Pitarke *et al.* and Esbenson and Sigmund in Ref. [5] within a many-body theoretical scheme, is expressed in terms of the first-order dielectric response function, which is evaluated with the full random-phase approximation (Lindhard dielectric function). Exchange effects, which were approximately included in Ref. [6] for low impact velocities, are not taken into account in the theory. We apply the model to the calculation of the energy lost by protons, antiprotons, and neutral hydrogen moving in aluminum. By examining differential

energy-loss distributions, some inconsistencies—such as negative probabilities at high transferred energies for antiprotons—are found in the theory. In consequence, we have modified the second-order term to get rid of such improper contributions.

In order to compare the theoretical values with experimental data, we add to the second-order stopping power due to collisions with the FEG the contribution coming from the interaction with electrons bound to target atoms. The energy loss originated by inner-shell ionization is evaluated with the continuum-distorted-wave–eikonal-initial-state (CDW-EIS) approximation [7,8], which includes all orders in Z_P, at least approximately. In the case of hydrogen, the existence of different exiting products is taken into account by weighing the stopping with the equilibrium charge-state fractions [9]. We also inspect the effect of the Z_P^3 term on the electronic density, comparing the results with those derived from the density-functional theory (DFT) [11].

The work is organized as follows. In Sec. II, we outline the model used, deriving the quadratic induced potential from a collisional point of view. Results are displayed and discussed in Sec. III, and in Sec. IV the conclusions are summarized. Atomic units are used except where indicated.

II. THEORY

Let us consider a heavy projectile (P) of charge Z_P moving with velocity $\mathbf{v}$ inside a solid, and colliding with the electrons of the FEG. Due to the large mass of the projectile, the description of its motion in terms of a classical trajectory is a reasonable approximation, with the projectile position at the time t given by $\mathbf{R}(t) = \mathbf{v}t$. We employ the time-dependent Hartree-Fock method to describe the electronic state of the FEG in the presence of the projectile. Within this formalism, the Schrödinger equation associated with the many-body problem can be described using the Hartree equations for the one-electron wave functions $\varphi_j(\mathbf{r},t)$ in the usual way:

$$[\hat{\mathbf{k}}^2/2+\mathcal{V}(\mathbf{r},t)]\varphi_j(\mathbf{r},t)=i\frac{\partial}{\partial t}\varphi_j(\mathbf{r},t), \qquad (1)$$

where $\hat{\mathbf{k}}=-i\boldsymbol{\nabla}_\mathbf{r}$ is the electron momentum operator,

$$\mathcal{V}(\mathbf{r},t)=u[\mathbf{r}-\mathbf{R}(t)]+\sum_{i=1}^{n}\int d\mathbf{r}'\,w(\mathbf{r},\mathbf{r}')|\varphi_i(\mathbf{r}',t)|^2 \quad (2)$$

is the self-consistent potential acting upon the jth electron (e), and j varies from 1 to n, with n the total number of electrons of the FEG (for more insight, see [12–14]). In the summation, the term $i=j$ should not be included, but for practical purposes, i.e., a large number of electrons, it has no relevance. In Eq. (2), the potential $u(\mathbf{r})=-Z_P/r$ (where $r=|\mathbf{r}|$) is the Coulomb P-e potential, $w(\mathbf{r},\mathbf{r}')=|\mathbf{r}-\mathbf{r}'|^{-1}$ describes the e-e interaction, and the exchange terms have been neglected. As $t\to-\infty$, the electronic states satisfy the asymptotic condition $\varphi_\mathbf{k}(\mathbf{r},t)\to\phi_\mathbf{k}(\mathbf{r})\exp(-iE_kt)$, where $\phi_\mathbf{k}(\mathbf{r})=(2\pi)^{-3/2}\exp(i\mathbf{k}\cdot\mathbf{r})$ is the unperturbed state, with energy $E_k=k^2/2$, of the jth electron, and the discrete index j has been replaced by the initial momentum $\mathbf{k}$.

Assuming an instantaneous response of the electrons to the projectile perturbation, the potential $\mathcal{V}(\mathbf{r},t)$ depends only on $\mathbf{r}-\mathbf{R}(t)$. Then, a formal solution of Eq. (1) is obtained by performing the Galilei transformation to the frame where the projectile is at rest, which is associated with the unitary operator $U(\mathbf{r},t)=\exp[-i(\mathbf{v}\cdot\mathbf{r}-t\mathbf{v}\cdot\hat{\mathbf{k}})]$. The transformed state

$$\Psi_\mathbf{k}(\mathbf{r},t)=U(\mathbf{r},t)\varphi_\mathbf{k}(\mathbf{r},t)$$

obeys the time-dependent Schrödinger equation for the Hamiltonian $H_e=\hat{\mathbf{k}}^2/2+V(\mathbf{r})$, where $V(\mathbf{r})=\mathcal{V}(\mathbf{r},t=0)$ is the perturbation located at the time origin. Since H_e does not depend on t, the solution $\Psi_\mathbf{k}(\mathbf{r},t)$ can be expressed as

$$\Psi_\mathbf{k}(\mathbf{r},t)=\psi'_\mathbf{k}(\mathbf{r})\exp(-iE_{k'}t),$$

where $\mathbf{k}'=\mathbf{k}-\mathbf{v}$ and $\psi_{k'}(\mathbf{r})$ is the stationary scattering state corresponding to the Hamiltonian H_e, which satisfies the boundary condition $\psi'_\mathbf{k}\to\phi'_\mathbf{k}$ as the perturbation vanishes (outgoing asymptotic condition).

As usual in atomic collisions, from the Lippmann-Schwinger equation we can derive a perturbative expansion of the stationary state $\psi'_\mathbf{k}$. By conserving terms up to the second order, we obtain

$$\psi'_\mathbf{k}=\phi'_\mathbf{k}+G_0^+V(\mathbf{r})\phi'_\mathbf{k}+G_0^+V(\mathbf{r})G_0^+V(\mathbf{r})\phi'_\mathbf{k}, \qquad (3)$$

where $G_0^+=(E_{k'}-\hat{\mathbf{k}}^2/2+i\eta)^{-1}$ (with $\eta\to0^+$) is the retarded Green function. As mentioned above, Eq. (3) is only a formal solution of the problem because the self-consistent potential $V(\mathbf{r})$ depends on the electronic states $\psi'_\mathbf{k}$, and therefore an iterative resolution is necessary. Employing the expansion given by Eq. (3), and introducing the Fourier transform $\tilde{V}(\mathbf{q})=\int d\mathbf{r}\exp(-i\mathbf{q}\cdot\mathbf{r})V(\mathbf{r})$, we obtain, after much algebra, an equation for the potential given by

$$\tilde{V}(\mathbf{q})\epsilon_L(\mathbf{q})=-Z_P\tilde{v}(\mathbf{q})+\tilde{v}(\mathbf{q})\rho_e\int d\mathbf{k}\Theta(k_F-k)$$

$$\times\int d\mathbf{p}\,f_2(\mathbf{k}';\mathbf{q},\mathbf{p})\tilde{V}(\mathbf{k}'+\mathbf{q}-\mathbf{p})\tilde{V}(\mathbf{p}-\mathbf{k}'),$$

$$(4)$$

where $\tilde{v}(\mathbf{q})=4\pi q^{-2}$, $\Theta(k_F-k)$ is the unitary Heaviside function that restricts the initial states to those contained inside the Fermi sphere (with k_F the Fermi velocity), $\rho_e=2$ takes into account the spin states, and $\mathbf{k}'=\mathbf{k}-\mathbf{v}$. The function $\epsilon_L(\mathbf{q})=1-\tilde{v}(\mathbf{q})\rho_e\int d\mathbf{k}\Theta(k_F-k)f_1(\mathbf{k}';\mathbf{q})$ is the well-known Lindhard dielectric function, with

$$f_1(\mathbf{k}';\mathbf{q})=(2\pi)^{-3}[g_0^+(\mathbf{k}'+\mathbf{q})+g_0^-(\mathbf{k}'-\mathbf{q})], \qquad (5)$$

$$f_2(\mathbf{k}';\mathbf{q},\mathbf{p})=(2\pi)^{-6}[g_0^+(\mathbf{k}'+\mathbf{q})g_0^+(\mathbf{p})$$

$$+g_0^-(\mathbf{k}'-\mathbf{q})g_0^-(\mathbf{p}-\mathbf{q})+g_0^+(\mathbf{p})g_0^-(\mathbf{p}-\mathbf{q})],$$

$$(6)$$

and $g_0^\pm(\mathbf{q})=(E_{k'}-E_q\pm i\eta)^{-1}$. In the derivation of Eq. (4), it is assumed that the total electric charge of the FEG is just neutralized by a uniform positive-charge background originating from the atomic cores.

The first-order potential $\tilde{V}^{(1)}(\mathbf{q})$ is derived by conserving only the first term on the right-hand side of Eq. (4), that is,

$$\tilde{V}^{(1)}(\mathbf{q})=-Z_P\tilde{v}(\mathbf{q})/\epsilon_L(\mathbf{q}). \qquad (7)$$

As any iterative solution, the second-order potential $\tilde{V}^{(2)}(\mathbf{q})$ is obtained by replacing Eq. (7) on the right-hand side of Eq. (4). After changing integration variables, it reads

$$\tilde{V}^{(2)}(\mathbf{q})=-Z_P\tilde{v}(\mathbf{q})/\epsilon_2(\mathbf{q}), \qquad (8)$$

where

$$\epsilon_2^{-1}(\mathbf{q})=\epsilon_L^{-1}(\mathbf{q})$$

$$\times\left[1-Z_P\rho_e\int d\mathbf{q}'\frac{\tilde{v}(\mathbf{q}-\mathbf{q}')}{\epsilon_L(\mathbf{q}-\mathbf{q}')}g(\mathbf{q},\mathbf{q}')\frac{\tilde{v}(\mathbf{q}')}{\epsilon_L(\mathbf{q}')}\right]$$

$$(9)$$

is the inverse of the quadratic dielectric response function $\epsilon_2(\mathbf{q})$, and $g(\mathbf{q},\mathbf{q}')=\int d\mathbf{k}\Theta(k_F-k)f_2(\mathbf{k}';\mathbf{q},\mathbf{k}'+\mathbf{q}')$ is the propagator. The potential $\tilde{V}^{(2)}(\mathbf{q})$ coincides with that derived by Pitarke et al. [5], and the function $g(\mathbf{q},\mathbf{q}')$ can be calculated analytically from Ref. [15]. Note that the linear-response function $\epsilon_L(\mathbf{q})$ is independent of the projectile charge; on the contrary, the response function $\epsilon_2(\mathbf{q})$ depends on Z_P.

A. Second-order stopping power

Within the DF, the second-order stopping power can be derived from the potential $\tilde{V}^{(2)}(\mathbf{q})$ as [16]

$$S_2^{DF} = -\frac{2Z_P^2}{\pi v^2}\int_0^{+\infty} d\omega\,\omega\int_{\omega/v}^{+\infty}\frac{dq}{q}\mathrm{Im}\left[\frac{1}{\epsilon_2(\mathbf{q})}\right],\qquad (10)$$

where $\omega=\mathbf{q}\cdot\mathbf{v}$ is the energy lost by the projectile. In the derivation of Eq. (10), we have explicitly used that $\epsilon_2(\mathbf{q})$ only depends on $q=|\mathbf{q}|$ and q_z with the z direction chosen parallel to $\mathbf{v}$. By using Eq. (9), S_2^{DF} reads

$$S_2^{DF}=S_1^{DF}+\frac{4Z_P^3}{\pi v^2}\int_0^{+\infty}d\omega\,\omega\int_{\omega/v}^{+\infty}\frac{dq}{q}$$

$$\times\mathrm{Im}\left[\frac{1}{\epsilon_L(\mathbf{q})}\int d\mathbf{q}'\frac{\widetilde{v}(\mathbf{q}-\mathbf{q}')}{\epsilon_L(\mathbf{q}-\mathbf{q}')}g(\mathbf{q},\mathbf{q}')\frac{\widetilde{v}(\mathbf{q}')}{\epsilon_L(\mathbf{q}')}\right],$$
$$(11)$$

where S_1^{DF} is the first-order stopping power, which is straightforwardly obtained from Eq. (10) by replacing ϵ_2 by ϵ_L. Note that the propagator $g(\mathbf{q},\mathbf{q}')$ depends explicitly on $\mathbf{v}$, while in the case of the first-order dielectric function, ϵ_L, the dependency on the projectile velocity is just contained in the variable ω.

The second term on the right-hand side of Eq. (11) represents the Z_P^3 term of the stopping power, which is sensitive to the sign of Z_P, while S_1^{DF} is proportional to Z_P^2. Thus, a good way of investigating second-order effects is to consider projectiles with opposite charge, i.e., protons and antiprotons; the difference between their stoppings is twice the Z_P^3 term.

B. Induced electron density

The induced electronic density can be derived from the quadratic potential $\widetilde{V}^{(2)}(\mathbf{q})$ by employing the Poisson equation, and it reads

$$n_2(\mathbf{r}')=\frac{-Z_P}{2\pi^2}\int_0^\infty dq\,q^2\int_0^1 d\omega'J_0[q\rho\sqrt{1-(\omega')^2}]$$

$$\times\{\cos(qz\omega')R-\sin(qz\omega')I\},\qquad(12)$$

where $\mathbf{r}'=(\rho,z)$ is the position vector measured from the projectile place, with ρ and z the cylindric coordinates with respect to $\mathbf{v}$, J_0 is the Bessel function of zero order, and $\omega'=q_z/q$, with q_z the component of $\mathbf{q}$ along the velocity direction. The functions R and I are defined in terms of the quadratic dielectric response $\epsilon_2(\mathbf{q})$ as

$$R=\mathrm{Re}\left[\frac{1}{\epsilon_2(\mathbf{q})}\right]-1,\qquad I=\mathrm{Im}\left[\frac{1}{\epsilon_2(\mathbf{q})}\right].\qquad(13)$$

As a consequence of the presence of the positive cores, which neutralize the total electronic charge, the total induced electronic charge inside the solid is null, i.e., $\int d\mathbf{r}'n_2(\mathbf{r}')=0$. The first-order induced electronic density $n_1(\mathbf{r}')$ can be calculated from Eq. (12) by replacing ϵ_2 by ϵ_L in Eq. (13).

C. Stopping of dressed projectiles

For ions carrying electrons, at high velocities it is possible to consider that the electrons bound to the projectile remain unperturbed during the collision. In this frozen approximation, the first-order potential is

$$\widetilde{V}_D^{(1)}(\mathbf{q})=-Z_P\frac{1}{\epsilon_L^D(\mathbf{q})}\widetilde{v}(\mathbf{q}),$$

where ϵ_L^D is the dressed Lindhard dielectric function, defined as $\epsilon_L^D(\mathbf{q})=\epsilon_L(\mathbf{q})/f(\mathbf{q})$, with $f(\mathbf{q})=1-F(\mathbf{q})/Z_P$. The function $F(\mathbf{q})$ is the well-known atomic form factor, and for projectiles containing electrons only in the K shell, it reads

$$F(\mathbf{q})=\sum_{n=1}^{n_p}\frac{(2z_n)^4}{(4z_n^2+q^2)^2},\qquad(14)$$

where n_p is the number of electrons in the $1s$ state ($n_p=1$ or 2), and z_n is the effective charge seen by the bound electron [17]. The second-order dressed potential reads

$$\widetilde{V}_D^{(2)}(\mathbf{q})=-Z_P\frac{1}{\epsilon_2^D(\mathbf{q})}\widetilde{v}(\mathbf{q}),\qquad(15)$$

where the dressed second-order dielectric function $\epsilon_2^D(\mathbf{q})$ is derived from Eq. (9) by replacing ϵ_L by ϵ_L^D, and it is

$$[\epsilon_2^D(\mathbf{q})]^{-1}=[\epsilon_L^D(\mathbf{q})]^{-1}\left\{1-Z_P^{-1}\rho_e\right.$$

$$\left.\times\int d\mathbf{q}'\,\widetilde{V}_D^{(1)}(\mathbf{q}-\mathbf{q}')g(\mathbf{q},\mathbf{q}')\widetilde{V}_D^{(1)}(\mathbf{q}')\right\}.$$
$$(16)$$

For H^0 projectiles, considered in the present work, in Eq. (14) $n_p=1$ and $z_n=1$.

III. RESULTS

We have confined our study to a system composed of singly charged or neutral projectiles ($H^+,\bar{p},H^0$) moving in aluminum solid, which can be considered as the prototype of the metal target. The parameters used to describe the aluminum are the following: the electron density is $N_e=0.0268$ (or equivalently the plasmon frequency $\omega_p=0.58$ and the Fermi velocity $k_F=0.927$), the atomic density $N_{at}=8.92\times10^{-3}$, and the inverse of the plasmon lifetime $\gamma^{-1}=0.037$ [18].

In Fig. 1, we plot the energy-loss distribution $S(\omega)\equiv dS/d\omega$ as a function of the lost energy ω for H^+, $\bar{p}$, and H^0 moving inside an aluminum solid target with velocity $v=1$ a.u. Second-order results $S_2^{DF}(\omega)$ are displayed with a solid line in Figs. 1(a) and 1(c), and with a dashed line in Fig. 1(b). The calculation of $S_2^{DF}(\omega)$ from Eq. (11) involves a three-dimensional integration on the momentum $\mathbf{q}'$ and a further integration on q, which were numerically done within an error of 1%. Values corresponding to the first-order energy loss $S_1^{DF}(\omega)$ are also plotted in Fig. 1 as a reference.
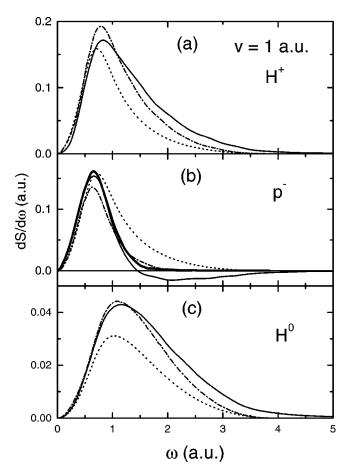
FIG. 1. Energy-loss distributions for 25 keV ($v=1$ a.u.) (a) protons, (b) antiprotons, and (c) neutral hydrogen on aluminum solid targets considering fixed-charge projectiles. Dotted line, the first-order contributions $dS_1^{DF}/d\omega$. Thin solid line, the second order $dS_1^{DF}/d\omega$. Thick solid line corresponds to "truncated" (nonnegative) second-order stopping $(dS_2')^{DF}/d\omega$. We compare with $dS_2^{BC}/d\omega$ of Ref. [1], dot-dashed line.

Because the impact velocity is lower than the threshold of plasmon excitation ($v < v_{thr} \simeq 1.2$ a.u.), the collective oscillations do not contribute to the energy loss. Therefore, the impact energy considered in Fig. 1 allows us to study in detail the behavior of the stopping produced by binary collisions with the FEG. For protons and neutral hydrogen, the maximum of the second-order distribution is higher than that corresponding to the first-order distribution, indicating an increment of the energy deposited in the solid by projectiles with positive charge with respect to predictions of the first order. For antiprotons, in contrast, the Z_P^3 term of the stopping power [second term of Eq. (11)] gives a negative contribution, and the energy-loss distribution $S_2^{DF}(\omega)$ exhibits values *lower than zero* for $\omega > 1.4$ a.u., as observed in Fig. 1(b). Such values, corresponding to negative probabilities, are clearly unphysical. To solve the serious problem that arises for $Z_P = -1$, in Eq. (11) we drop the negative probabilities by replacing the negative values of $dS_2^{DF}(\omega)/dq$ by $dS_2^{DF}(\omega)/dq = 0$. This prescription is equivalent to defining a second-order stopping $(S_2')^{DF}$ by introducing $\Theta(\text{Im}[-1/\epsilon_2(\mathbf{q})])$ in the integrand of Eq. (10), that is,

$$(S_2')^{DF} = -\frac{2Z_P^2}{\pi v^2} \int_0^{+\infty} d\omega\, \omega \int_{\omega/v}^{+\infty} \frac{dq}{q}$$

$$\times \text{Im}\left[\frac{1}{\epsilon_2(\mathbf{q})}\right] \Theta\left(\text{Im}\left[\frac{-1}{\epsilon_2(\mathbf{q})}\right]\right). \qquad (17)$$

Note that this new definition only affects the second-order energy loss for negative values of Z_P, leaving unchanged the results for neutral and positive projectiles. Values of $(S_2')^{DF}(\omega)$ are plotted in Fig. 1(b) by a solid line, and they are lower than $S_1^{DF}(\omega)$ in the range of high lost energies. The modification introduced in Eq. (17) breaks the symmetry of proton and antiproton results with respect to first-order stopping power. Since such symmetry is characteristic of the Z_P^3 term, it is expected that the elimination of negative probabilities incorporates, in some approximate way, terms of higher order in Z_P in the energy loss.

With the purpose of testing the validity of the Eq. (17), we compare the results of $(S_2')^{DF}(\omega)$ with the second-order values $S_2^{BC}(\omega)$, calculated within the BCF [4], which are also plotted in Fig. 1 (dot-dash line). As for $v = 1$ a.u., the plasmon mechanism is not present in the energy-loss process; the DF and BCF first-order distributions are equal, as was shown in [1]. Some differences might, however, appear in the second-order contributions because the DF can involve excited plasmon states as intermediate states, while these virtual collective states are not contained in the BCF. And this should be the reason why the distribution $(S_2')^{DF}(\omega)$ extends beyond $\omega = 2v(v + k_F)$, which is the maximum allowed value of lost energy in a single-particle collision. A good agreement between the second-order energy-loss distributions $(S_2')^{DF}(\omega)$ and $S_2^{BC}(\omega)$ is observed in Fig. 1, which supports the effectiveness of the modification included in Eq. (17). On the other hand, several kinds of Padé approximants were tried with no success in getting rid of the negative values of the second-order probability in the DF.

In Fig. 2, we show the energy-loss distribution $S^{DF}(\omega) \equiv dS^{DF}/d\omega$ for H$^+$, $\bar{p}$, and H^0 moving with $v = 2$ a.u. in aluminum. At this impact velocity, the plasmon excitation mechanism can contribute to the energy loss. For protons and antiprotons, a sharp peak at $\omega \sim \omega_p$ is displayed in the first- and second-order distributions, and such a peak corresponds to the energy lost by plasmon excitation processes. In the case of neutral hydrogen, in contrast, the incident atom cannot excite collective modes due to the short range of the projectile potential [1], and the energy-loss distribution is broader, with no visible footprints of the plasmon mechanism. By comparing Figs. 2(a) and 2(b) for $\omega \gtrsim \omega_p$, it is found that antiprotons cancel a significant portion of the energy distribution, while protons reinforce it. In other words, antiprotons avoid head-on collisions involving high-energy transfer, but these collisions are strengthened for proton impact. In Fig. 2(b), the curves corresponding to $S_2^{DF}(\omega)$ and the modified version $S_2'^{DF}(\omega)$ seem to be similar; however, remarkable differences are observed in the amplified vision displayed in Fig. 3. For antiprotons at $v = 2$ a.u., negative values of $S_2^{DF}(\omega)$ for high lost energies are also observed.
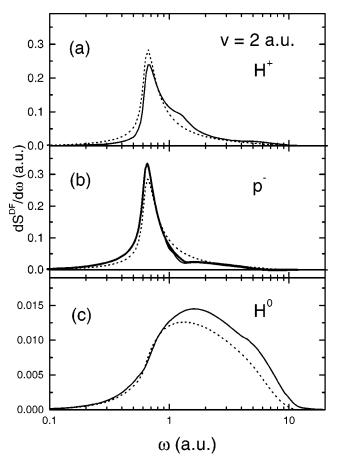
FIG. 2. Energy-loss distributions for 100 keV ($v = 2$ a.u.) (a) protons, (b) antiprotons, and (c) neutral hydrogen on aluminum solid targets considering fixed-charge projectiles. Dotted line, the first-order contributions $dS_1^{DF}/d\omega$. Thin solid line, second order $dS_2^{DF}/d\omega$. Thick solid line corresponds to "truncated" (non-negative) second order stopping $(dS_2')^{DF}/d\omega$.

FIG. 3. Magnification for transferred high energy of energy-loss distributions (Fig. 2) for H^+ and $\bar{p}$.

Although at this impact velocity the negative contribution to the stopping power is not meaningful, the presence of negative probabilities affects the calculation of the total energy loss. Notice that the unphysical behavior of $S_2^{DF}(\omega)$ for high values of ω is not an exclusive characteristic of small velocities, but it persists for high impact energies.

Figure 4 displays stopping power per unit length, as a function of the projectile velocity, for protons [Fig. 4(a)], antiprotons [Fig. 4(b)], and neutral hydrogen [Fig. 4(c)] moving through aluminum. The results for H^+ projectiles coincide with those calculated by Pitarke *et al.* [5], although a different value of γ is considered. From the figure it is observed that the Z_P^3 term increases the first-order prediction for H^+ and H^0, while for $\bar{p}$ the second-order term lowers it. At small velocities, all results tend linearly to zero.

So as to compare the theoretical results with experimental data, we calculate the total stopping power S_2 as

$$S_2 = (S_2')^{DF} + S_{CDW-EIS}^{IS}, \qquad (18)$$

where $S_{CDW-EIS}^{IS}$ represents the stopping due to inner-shell ionization of the solid atoms. The $S_{CDW-EIS}^{IS}$ contribution is
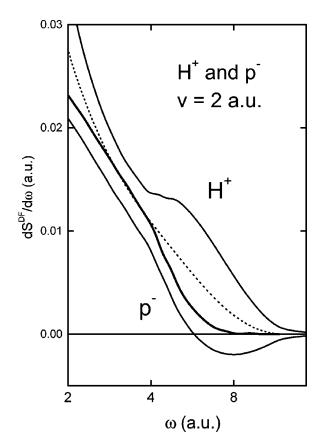
calculated using the CDW-EIS approximation, which includes all orders on Z_P, at least approximately [8]. The initial bound states are described with Hartree-Fock double-Z functions [19] corresponding to the ion Al^{3+}, while a Coulomb wave function with a charge satisfying the binding energy is used to describe the final continuum state. In Fig. 5, we show S_2 as a function of v for hydrogen and antiprotons. As in previous figures, we also plot the first-order total stopping power, calculated as $S_1 = S_1^{DF} + S_{CDW-EIS}^{IS}$. In the case of hydrogen, the different charge states of the projectile are taken into account by weighing their partial contributions with the equilibrium fractions. In the results of total stopping power, we neglected the contributions of H^-. The energy loss due to projectile charge-exchange processes has also been neglected in our calculation. The contributions coming from capture from the FEG and atomic inner shells have been estimated to be lower than 10% [9] and 1% [10], respectively, for the velocities considered here. For H projectiles at high impact velocities, the agreement with experiments is good, but discrepancies have been observed below $v = 1.7$ a.u. At these intermediate velocities, the second-order stopping S_2 overestimates the experimental values, whereas S_1 underestimates them. For antiprotons, in contrast, S_2 results agree with the experiments at intermediate energies, except a small depression at $v = 1.2$ a.u., and they quickly tend to the first-order values as v increases, running above experimental data in the high-energy range. The velocity $v = 1.2$ a.u., where the dip in the antiproton results
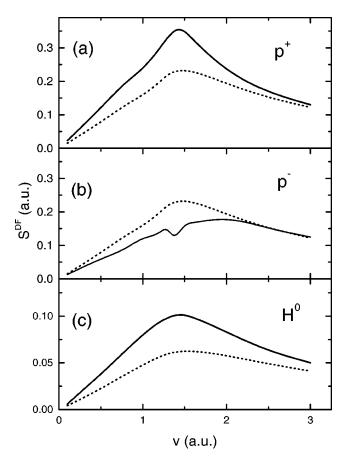
FIG. 4. Stopping power, for (a) protons, (b) antiprotons, and (c) neutral hydrogen on aluminum solid targets as a function of the impact velocity, considering the projectile charge as fixed. Dotted line, the first-order contributions $dS_1^{DF}/d\omega$. In (a) and (c), the solid line denotes the second-order stopping power $dS_2^{DF}/d\omega$. In (b), the solid line corresponds to "truncated" (non-negative) second-order stopping $(S_2')^{DF}$.
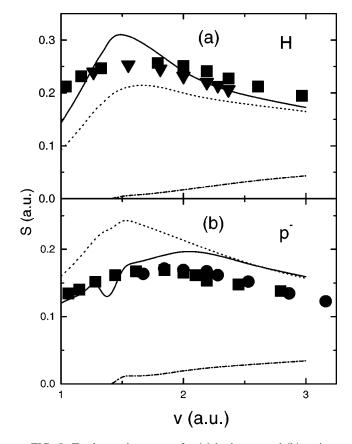

FIG. 5. Total stopping power for (a) hydrogen and (b) antiprotons on an aluminum solid target as a function of the impact velocity. Dotted line, total first-order stopping $S_1(H)$ and $S_1(\bar{p})$; and dot-dashed line, stopping due to ionization of inner shell $2s$ and $2p$ calculated with the CDW-EIS approximation. (a) Solid lines, total second-order stopping $S(H)$; (b) solid line accounts for corrected (non-negative) second-order stopping $S(H)$. Symbols represent the experiments for hydrogen (Refs. [21–23]) and antiprotons (Ref. [24]).

appears, corresponds to the threshold of collective contributions, and the depression in the S_2 curve for antiprotons can be associated with the second-order hump present in H$^+$ calculations [5]. Of course, these structures of the stopping power do not seem to have physical meaning.

Finally, by using the second-order model, we have investigated the electronic density induced by the projectile in the FEG [20]. For H$^+$ and $\bar{p}$ moving with $v=0.8$ a.u. in an aluminum FEG, the electronic density $n_2(\mathbf{r'}=z\hat{\mathbf{z}})$ calculated from Eq. (12) and normalized with the unperturbed electronic density N_e has been plotted in Fig. 6 as a function of the distance z to the projectile position. We also display proton and antiproton results calculated by Salin using the DFT [11]. In that calculation, the exchange correlation contribution was neglected according to our model, but the values do not differ considerably from the ones accounting for exchange. The induced electronic density $n_1(\mathbf{r'}=z\hat{\mathbf{z}})$ derived from $\widetilde{V}^{(1)}(\mathbf{q})$ is also shown in Fig. 6. As the first-order potential depends linearly on Z_P, the n_1 values for protons and antiprotons coincide in modulus, only differing in sign. The first-order model fails drastically in reproducing the density

provided from the DFT, especially for antiprotons where $n_1(\mathbf{r'}=z\hat{\mathbf{z}})/N_e<-1$ near the origin. The second-order values correct, in some way, the failure of the first order n_1. For H$^+$, the results of n_2 agree qualitatively with the DFT data, although for $\bar{p}$ the second-order n_2 incorporates an undesirable positive enhancement, precisely in the antiproton position. By inspecting the behavior of the electronic density n_2 in the $\mathbf{r'}$ space, it is possible to map the region (q,ω) in the momentum space where ϵ_2 fails. From Eq. (12), at the projectile position ($\mathbf{r'}=\mathbf{0}$) the electronic density n_2 only depends on the function R, being independent of the function I. Therefore, for $Z_P=-1$, values of $R>0$ are associated with positive values of the density at the position $\mathbf{r'}=\mathbf{0}$, as observed in Fig. 6. Then, we introduce a similar criterion to the one used in Eq. (17) to avoid the improper positive electronic density for antiprotons. We include the Heaviside function $\Theta(1-\mathrm{Re}[1/\epsilon_2(\mathbf{q})])$ in the definition of the function R given by Eq. (13), and the modified function R' reads

$$R' = \left(\mathrm{Re}\left[\frac{1}{\epsilon_2(\mathbf{q})}\right]-1\right)\Theta\left(1-\mathrm{Re}\left[\frac{1}{\epsilon_2(\mathbf{q})}\right]\right). \qquad (19)$$
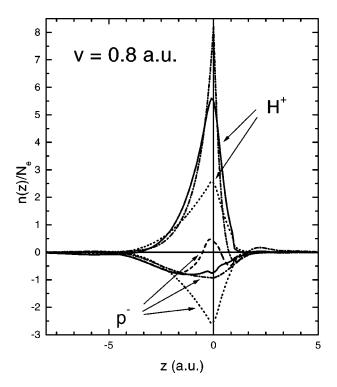
FIG. 6. Induced relative density $n(z)/N_e$ of electrons for $v = 0.8$ a.u. protons and antiprotons in the direction of the projectile as given by Eq. (12). Dotted line, first Born approximation; second Born approximation for antiprotons denoted by the dashed-line and for protons by the solid line; second Born approximation for antiprotons with additional conditions (see body of text) denoted by the solid line dot-dashed line denotes calculations of Salin [11] using DFT.

Results of n_2 calculated by using R' are shown with a solid line in Fig. 6 for $\bar{p}$ projectiles. Again note that the modification introduced in Eq. (19) does not change the results for protons, while for antiprotons the new values of n_2 now approach very close to the DFT predictions [11]. The difference between n_2 and DFT results at $z=0$ can be easily explained as a consequence of our using a finite lifetime γ^{-1}, while in the DFT an infinite lifetime is considered.

Summing up, in the energy-loss distribution and the induced electronic density, two different problems were individualized in the second-order theory given by Eq. (8). These problems are corrected here through Eqs. (17) and (19), respectively.

IV. CONCLUSIONS

We study stopping of heavy projectiles moving in a FEG within the DF, conserving terms up to second order in Z_P. The obtained quadratic wake potential, which was previously calculated by Pitarke *et al.* and Esbensen and Sigmund [5], is expressed in terms of the full random-phase approximation or Lindhard dielectric function. The model is applied to the calculation of the energy-loss distribution for protons, neutral hydrogen, and antiprotons moving through aluminum. In the case of antiprotons, negative probabilities for high transferred energy are found in the theory, and these unphysical probabilities are present for all impact velocities. We propose a modification of the second-order stopping power to avoid negative probabilities. The new expression $(S_2')^{\text{DF}}$, given by Eq. (17), incorporates in some undetermined way higher-order terms in Z_P, and therefore it breaks the proton-antiproton symmetry of second-order results with respect to first-order values. Results obtained with the proposed second-order DF describe properly the difference between proton and antiproton stopping; protons deposit more energy in the high-energy tail, while, on their part, antiprotons diminish their contribution.

For hydrogen and antiproton projectiles, the total stopping power is calculated by adding to FEG results the contribution coming from the inner-shell ionization, which is evaluated with the CDW-EIS approximation. For incident H, theoretical results involving the different equilibrium charge states of the projectile agree with experimental data at high velocities. Instead, for $\bar{p}$ the second-order values overestimate the experiments as v increases.

By employing the second-order model, we also investigate the induced electronic density. Some inconsistencies were again found for antiprotons, and they were solved by using a modified version of the electronic density. For both protons and antiprotons, the obtained electronic density is in very good agreement with the values derived from the DFT.

[1] D.G. Arbó and J.E. Miraglia, Phys. Rev. A **58**, 2970 (1998).

[2] P. Sigmund, Phys. Rev. A **26**, 2497 (1982).

[3] P.M. Echenique, F. Flores, and R.H. Ritchie, Solid State Phys. **43**, 229 (1990), and references within.

[4] D.G. Arbó, M.S. Gravielle, and J.E. Miraglia, Phys. Rev. A **62**, 032901 (2000).

[5] J.M. Pitarke, R.H. Ritchie, and P.M. Echenique, Phys. Rev. B **52**, 13 883 (1995); J.M. Pitarke, R.H. Ritchie, P. Echenique, and E. Zaremba, Europhys. Lett. **24**, 613 (1993); H. Esbensen

and P. Sigmund, Ann. Phys. (N.Y.) **201**, 152 (1990).

[6] T. del Río Gaztelurrutia and J.M. Pitarke, Phys. Rev. B **62**, 6862 (2000).

[7] D.S.F. Crothers and J.F. McCann, J. Phys. B **16**, 3229 (1983).

[8] P.D. Fainstein, V.H. Ponce, and R.D. Rivarola, J. Phys. B **24**, 3091 (1991).

[9] M. Peñalba, A. Arnau, P.M. Echenique, F. Flores, and R.H. Ritchie, Europhys. Lett. **19**, 45 (1992).

[10] The contribution of capture from the L shell of Al, calculated

with the eikonal impulsive approximation, is one order of magnitude less than inner-shell ionization, i.e., for $v=2$ it is 1.94×10^{-3} a.u.

[11] A. Salin (private communication); A. Salin, A. Arnau, P.M. Echenique, and E. Zaremba, Phys. Rev. B **59**, 2537 (1999).

[12] N.W. Ashcroft and N.D. Mermin, *Solid State Physics* (Holt, Reinhart and Winston, New York, 1976).

[13] J.P. Blaizot and G. Ripka, *Quantum Theory of Finite Systems* (The MIT Press, Cambridge, 1986).

[14] A. Szabo and N.S. Ostlund, *Modern Quantum Chemistry: Introduction to Advanced Electronic Structure Theory* (Macmillan Publishing Co., New York, 1982).

[15] R. Cenni and P. Saracco, Nucl. Phys. A **487**, 279 (1988).

[16] J. Lindhard and A. Winther, K. Dan. Vidensk. Selsk. Mat. Fys. Medd. **34**, No. 4 (1964).

[17] R.A. Bonham and D.A. Kohl, J. Chem. Phys. **45**, 2471 (1976).

[18] N.R. Arista and A.F. Lifschitz, Phys. Rev. A **59**, 2719 (1999).

[19] E. Clementi and C. Roetti, At. Data Nucl. Data Tables **17**, 332 (1974).

[20] A. Bergara, I. Campillo, J.M. Pitarke, and P.M. Echenique, Phys. Rev. B **56**, 15 654 (1997).

[21] J.H. Ormrod and H.E. Duckworth, Can. J. Phys. **41**, 1424 (1963); J.H. Ormrod, J.R. MacDonald, and H.E. Duckworth, *ibid.* **43**, 275 (1965).

[22] W. White, J. Appl. Phys. **38**, 2660 (1967).

[23] S. Kreussler, C. Varelas, and R. Sizmann, Phys. Rev. B **26**, 6099 (1982).

[24] S.P. Moller, *et al.*, Phys. Rev. A **56**, 2930 (1997).